Optics Letters

Architecture for integrated RF photonic downconversion of electronic signals

Nathan P. O'Malley,[1,*] Keith A. McKinzie,[1] Mohammed S. Alshaykh,[1,2] Junqiu Liu,[3] Daniel E. Leaird,[1,4] Tobias J. Kippenberg,[3] Jason D. McKinney,[1,5] and Andrew M. Weiner[1]

[1]Elmore Family School of Electrical and Computer Engineering, Purdue University, West Lafayette, Indiana 47907, USA
[2]Electrical Engineering Department, King Saud University, Riyadh 11421, Saudi Arabia
[3]Institute of Physics, Swiss Federal Institute of Technology Lausanne (EPFL), CH-1015 Lausanne, Switzerland
[4]Currently with Torch Technologies, supporting AFRL/RW, Eglin Air Force Base, Florida, USA
[5]Formerly with U.S. Naval Research Laboratory, Washington, DC 20375, USA
*Corresponding author: omalleyn@purdue.edu

Received 1 September 2022; revised 14 October 2022; accepted 8 November 2022; posted 9 November 2022; published 23 December 2022

Electronic analog to digital converters (ADCs) are running up against the well-known bit depth versus bandwidth trade off. Towards this end, radio frequency (RF) photonic-enhanced ADCs have been the subject of interest for some time. Optical frequency comb technology has been used as a workhorse underlying many of these architectures. Unfortunately, such designs must generally grapple with size, weight, and power (SWaP) concerns, as well as frequency ambiguity issues which threaten to obscure critical spectral information of detected RF signals. In this work, we address these concerns via an RF photonic downconverter with potential for easy integration and field deployment by leveraging a novel, to the best of our knowledge, hybrid microcomb/electro-optic comb design.

https://doi.org/10.1364/OL.474710

Increasing demand for high-speed data transmission and processing has helped motivate the development of electronic analog to digital converters (ADCs) at impressive speeds. Unfortunately, progress in ADCs seems to be challenged by the well-known bit-depth versus bandwidth trade off [1]. Technical issues with timing jitter often take a toll, and as transmission rates increase, so does comparator ambiguity [1]. A range of radio frequency (RF) photonic solutions have been proposed that vary in implementation [2–7], but are generally united by their use of optical frequency combs. These combs possess extremely high frequency stability, and so promise to correct for some of the timing inaccuracies that plague electronic solutions at high frequencies. Demonstrations of RF photonic downconverters illustrate the power of optical frequency combs for sampling broadband electronic signals. However, in order to be deployed in real-world scenarios, optimization of size, weight, and power (SWaP) ought to be considered. Of the typical frequency comb generation methods, mode locked lasers are perhaps the most common, but cascaded electro-optic (EO) modulators are also frequently used. Both approaches can often be rather expensive from a SWaP perspective—commercially available mode locked lasers often have electrical-to-optical power conversion efficiencies of a few percent at most, with average optical powers at or above a few 100 milliwatts [8], suggesting electrical power draws of at least several Watts, often significantly more. Volumes of several liters are a typical lower bound. General SWaP metrics for EO comb generators are difficult to estimate due to the variety of implementations. However, as an example, a typical EO comb generator used in our laboratory requires powers and volumes roughly comparable with those of mode-locked lasers [9]. This uses discrete optical components, but improved SWaP is possible with on-chip technologies such as lithium niobate on insulator (LNOI) modulators. A recent impressively low-power result (though having too few comb lines for the work presented in this Letter) still required more than 3 W of RF power [10].

Additionally, in many works on photonic downconversion, the photonic component of the system functions as a channelizing front end, splitting a broad input spectrum into slices and sending each slice to a separate electronic detector (see for example [3]). This approach is necessary when signals with bandwidths spanning multiple Nyquist bands are targeted. In certain analog applications, e.g., dual band radar, the signals of interest have center frequencies covering multiple Nyquist bands but bandwidths contained within a single Nyquist band. In such cases, the use of many parallel detectors is not strictly necessary and a single detector could suffice, simplifying the system. We especially target such applications here. However, due to Nyquist folding, in this scheme spectral information would be lost and the input signal's original frequency would be unknown after downconversion. Disambiguation techniques are required to recover this information, critical for applications such as electronic support and signals intelligence [11].

In this work, we demonstrate a dual-comb architecture for photonic downconversion of wideband RF signals with potential for eventual on-chip integration. We accomplish this by taking advantage of maturing silicon nitride microcomb technology for one of our two combs. Silicon nitride (SiN) resonators have been used to generate coherent soliton frequency combs on-chip for nearly a decade [12]. The platform is CMOS foundry compatible and has been used to generate frequency combs

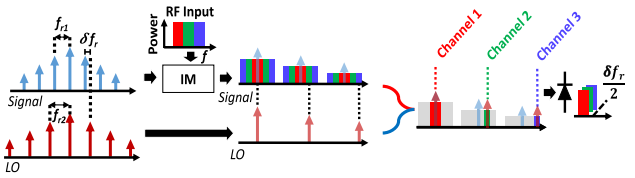

Fig. 1. Diagram of dual comb approach for downconversion. LO comb lines each sample different portions of the RF input spectrum, thus folding the spectrum down to a $\delta f_r/2$-wide baseband region.

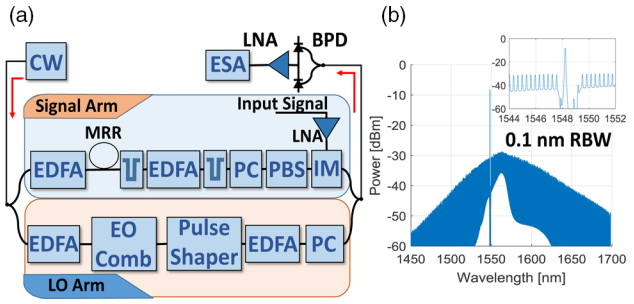

Fig. 2. (a) Experimental setup: CW, continuous wave laser; MRR, microring resonator; PC, polarization controller; PBS, polarizing beam splitter; IM, intensity modulator; BPD, balanced photodetector; ESA, electrical spectrum analyzer. (b) Optical spectrum of the soliton after the pump is partially notched by the filter after the ring. The EDFA's gain spectrum is visible from ~ 1530–1620 nm. The inset is a close-up of the comb near the pump, showing individual comb lines spaced at ~ 40 GHz, as well as the spectral notching of the optical filter.

with milliwatt levels of input optical power [13]. Generally soliton microcombs require an off-chip pump source to drive the SiN microring. However, within the last few years, optical pump sources have been successfully integrated for soliton generation powered by an AAA battery [14] and even for heterogeneously integrated on-chip pump/microring pairs [15], suggesting convenient deployment of microcombs into the field may be approaching in the near future.

While the SiN-based microcomb is very attractive from a SWaP perspective, the power per comb mode is limited by characteristically poor pump-to-sideband conversion efficiency [16]. Thus, we utilize an EO comb as our secondary comb, here termed the local oscillator (LO) comb. The EO comb can provide much higher power per comb mode than a soliton microcomb, which can in turn lead to improved system RF gain. Additionally, the EO comb uniquely addresses another of the concerns with some previous RF downconverters—namely, the issue of spectral ambiguity. Our hybrid EO comb/microcomb system—to our knowledge, a first-of-its-kind demonstration—allows for the use of a single detection stage (rather than many in parallel) to acquire the entire input spectrum while also overcoming the challenge of input frequency band ambiguity. This is accomplished through disambiguation techniques leveraging the easy tunability of the EO comb repetition rate.

Our approach is outlined in Fig. 1, and is related to works such as Refs. [3–5]. The soliton "signal" comb has a repetition rate f_{r1}, and passes through a null-biased intensity modulator by which the RF signal of interest is inscribed onto the comb. Each comb mode inherits a spectral copy of the input RF spectrum. Note that since dual combs are used for downconversion, it is the mixing of the combs' electric field terms—rather than a single comb's intensity—that is of importance. Thus, the null bias point is appropriate rather than the quadrature bias often used in direct detection systems [17]. The LO comb has a repetition rate of $f_{r2} = f_{r1} + \delta f_r$. When the two combs beat together on a photodetector, the different LO comb modes sample the input RF spectrum in chunks of bandwidth δf_r (one so-called "Nyquist zone" of width $\delta f_r/2$ on either side of each LO line) and fold them all down to a common baseband region from DC to $\delta f_r/2$. This sampling of the RF spectrum is a result of the two combs' slightly offset repetition rates, and allows a system with bandwidth equal to that of the Nyquist zone width (rather than the full input spectral width) after the photonic downconverter to process the signal(s) of interest.

We implement this structure as in Fig. 2(a). An external cavity diode laser (ECDL) around 1550 nm is split into two arms, one for each comb. In the signal arm (soliton comb), an erbium-doped fiber amplifier (EDFA) amplifies the laser before it is coupled on-chip via lensed fibers. Additionally, we rotate the polarization of the laser to properly align with the waveguides on chip. We utilize an ultrahigh-Q microring [free spectral range (FSR) ~ 40.374 GHz] from a batch featuring average loaded and intrinsic Qs of over 10^7 each, fabricated using the photonic Damascene process [18]. This high Q lowers the required pump power for comb generation and allows for reduced thermal effects in the microring—effects that often plague soliton generation. Rather than using a complex generation scheme as is often required, we tune our laser from blue to red across a microring resonance until solitons are generated, and back-detune to reach a single soliton [19]. An optical spectrum analyzer (OSA) trace of the soliton's optical spectrum is shown in Fig. 2(b). The strong pump line [here attenuated by a dense wavelength division multiplexing (DWDM) functioning as a notch filter] is immediately visible above the weaker comb lines. A second EDFA and DWDM-notch filter increase the total comb power while reducing the relative pump power. The RF signal input is sent through an electrical low-noise amplifier (LNA) and modulated onto the signal comb using an optical intensity modulator (IM).

The LO arm (EO comb) begins similarly, in this case with an EDFA amplifying the ECDL before the optical carrier passes through the EO comb generator. This portion of our system has been explained elsewhere [9]. In short however, a series of optical phase modulators and an intensity modulator are used to modulate the input CW laser, generating a flattop, broadband optical frequency comb with ~ 55 lines within its 3 dB bandwidth. Due to the limited RF bandwidth of the modulators used to generate the EO comb, we use a tunable RF signal generator to set the comb's repetition rate at ~ 14.266 GHz, just over one third of the soliton repetition rate. Accordingly, every third EO comb line is situated relatively close to a soliton line and can participate in downconversion. This effectively multiplies the EO comb repetition rate by three to $3 \times 14.266 = 42.798$ GHz. This is ~ 2.42 GHz higher than the soliton repetition rate, fixing $\delta f_r = 2.42$ GHz and the Nyquist bandwidth at 1.21 GHz. A commercial pulse shaper is used to select desired lines from the EO comb. For the experiments reported here, we only allow one LO line from the EO comb to pass at any given time, thus demodulating only two corresponding Nyquist bands. Alternatively, the spectral filter could be configured to allow only every third EO comb line to pass, which would provide for downconversion of multiple RF bands simultaneously. The presence of multiple LO lines would increase shot noise, but due to large link loss (to be

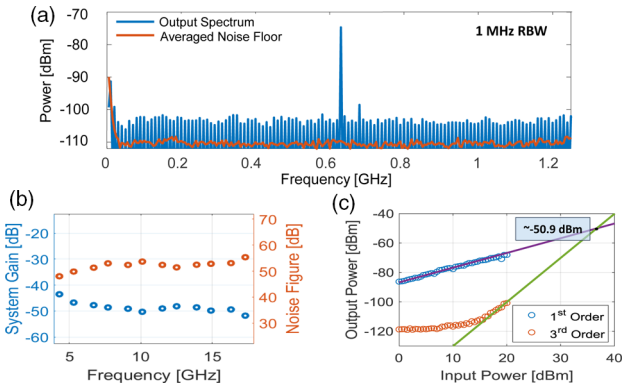

Fig. 3. (a) Sample system output RF spectrum. A small extraneous spur is seen around 675 MHz. The video-averaged system output noise floor is also shown. (b) System gain and NF metrics. (c) Two-tone test of the photonic portion of the system (without the pre-IM LNA) is conducted with RF inputs at ~ 11.5 GHz.

discussed shortly) our system is not shot noise limited, so this is not expected to significantly degrade our system performance.

After the pulse shaper, an EDFA amplifies the remaining EO comb lines, which are then polarization-rotated to match the polarization of the signal comb before detection on a balanced photodetector. An LNA chain is used to resolve the system noise floor above our ESA's instrument noise floor, but in a real-world application these would not be required, and the chain gain and noise figure (NF) have been removed from the results reported here. This subtraction may be contributing to the low-frequency feature seen in the system output [see Fig. 3(a)], as one of our LNAs cuts off below ~ 50 MHz.

Our system supports input RF signals from ~ 3.6 GHz to ~ 18 GHz, limited on the low side by our optical pump notch filters and on the high side by the bandwidth of our pre-IM LNA. We test our system performance by using single sinusoidal tones at various frequencies throughout the operating band. A summary of results can be seen in Figs. 3(a) and 3(b). Figure 3(a) is a trace taken from our ESA at 1 MHz resolution bandwidth (RBW) with an 11.5 GHz RF tone input to the system. It is downconverted to the expected ~ 600 MHz, maintaining a ~ 35 dB SNR at 1 MHz RBW (~ 4 dB SNR integrated over the 1.21 GHz Nyquist bandwidth, of note for ADC applications) with relatively limited RF input power around −30 dBm. A summary of metrics across the bandwidth of our system can be seen in Fig. 3(b). The photonic link's gain ranges from −44 dB to −51 dB over its operating bandwidth. The noise figure ranges from 48 dB to 55 dB. These gain/NF values are calculated by standard cascade analysis [20] using measured gain and specified noise figure of the pre-IM LNA and measured gain and noise figure of the photonic link. The loss of the photonic portion of the system (roughly −80 dB) strongly dominates the gain of our pre-IM LNA (Gain ~ 33 dB, noise figure ~ 2.4 dB), resulting in a significant noise figure attributed predominantly to the system loss. The aforementioned low conversion efficiency of the microcomb is certainly a contributing factor here. The LO comb line (measured before the final 2×2 coupler and BPD) for most of the channels tested is ~ −10 dBm with an optical signal-to-noise ratio (OSNR) of ~ 30 dB at 0.1 nm RBW on the OSA. We estimate the signal comb line power before (after) the second EDFA in the signal arm is ~ −32 dBm (~ −5 to −10 dBm) with a ~ 13 dB (~ 6 dB) OSNR at 0.1 nm RBW.

After testing with single sinusoidal tones, we perform two-tone measurements of our pre-IM LNA and the rest of the photonic link separately in order to identify their individual output third-order intercept points (OIP_3), a standard metric for quantifying nonlinearity in RF systems [21]. Seen in Fig. 3(c) is a measurement of the optical system with input tones around 11.5 GHz. The OIP_3 is measured to be roughly −50.9 dBm, determined from fixed-slope linear fits to the log-scale data as shown. The LNA OIP_3 is measured separately to be ~18.4 dBm. A standard cascade analysis [20] reveals a computed total system OIP_3 of ~ −58 dBm with an 11.5 GHz input signal, again strongly limited by the photonic portion of the system, and again expected in a photonic system with relatively low comb powers. As a last step in analyzing the system's RF metrics, we use the measured noise and OIP_3 seen in Fig. 3(c) to estimate the spur-free dynamic range (SFDR) of our system. We use the standard definition of $SFDR_3 = (OIP_3/N_{out})^{2/3}$ [21], and observe N_{out} as ~ −170 dBm/Hz by examining the video-averaged noise floor in Fig. 3(a), where the video averaging serves to smooth the noise floor for easier estimation of SNR without altering the noise level. We thereby estimate $SFDR_3 \approx 74.6$ dB/Hz$^{2/3}$. There are several promising options for further advancing the system performance metrics, which will be addressed in detail shortly.

As all of the input spectrum's $\delta f_r/2$-wide Nyquist zones are folded down into a single common $\delta f_r/2$-wide band at the output, one cannot immediately discern a signal's originating Nyquist zone simply by detecting it at the output. This could be overcome by either limiting the allowed RF input frequencies (not desirable, as it would artificially limit the system bandwidth) or by using many parallel photodetector + ADC pairs after the downconverter (eg, [6]). In this work, we leverage the easy tunability of our EO comb repetition rate to perform disambiguation [22]. As the EO comb repetition rate is shifted, the downconverted output signal also shifts accordingly. Critically, the shift of the output signal is proportional to the product of the EO comb repetition rate shift and the mode number of the EO comb line relative to the CW pump, allowing the output frequency shift to reveal the originating Nyquist zone of the signal and thereby its frequency. Experimentally, we perform this by simple tuning of the RF signal generator (Agilent E8257D) with a settling time of <10 ms. More generally, an RF voltage-controlled oscillator (VCO) can be used for faster (potentially sub-microsecond) tunability. However, the VCO's phase noise must be considered as it can affect the SNR performance [23]. The magnitude of this frequency shift sets a limit on the acquisition time or frequency resolution bandwidth when using an ADC or ESA, respectively, and must be large enough to accommodate the input signal bandwidth.

This technique is tested separately with signals at twelve different input Nyquist zones—six are "low" Nyquist zones (Nyquist bands immediately at the low-frequency side of their respective LO line), and six are at "high" Nyquist zones (bands at higher frequency than their LO line). Importantly, low and high Nyquist zones are distinguished by the direction of the output signal frequency shift when the EO comb repetition rate is changed. This is a key benefit of our system, as this kind of Nyquist zone distinguishing is often accomplished via coherent detection (e.g., Ref. [24]) but here requires only a single BPD. The results of this technique with the six high Nyquist bands are shown in Fig. 4(a). After disambiguation, the input frequencies are recovered; our results match the actual input frequencies

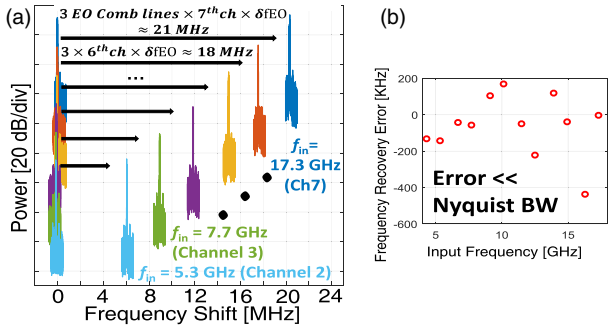

Fig. 4. (a) Demonstration of disambiguation. On the left-hand side, six test signals are separately downconverted to the baseband Nyquist zone. After the EO comb repetition rate is shifted by 1 MHz, the downconverted input at 5.3 GHz shifts by roughly 6 MHz while a downconverted 7.7 GHz signal shifts by 9 MHz, and so on. (b) Recovered signal frequency error.

(measured separately on an ESA) with only a few hundred kilohertz of error, as seen in Fig. 4(b). We believe this error may be due to minor drifting in the free-running soliton repetition rate, but regardless is much smaller than the Nyquist bandwidth (1.21 GHz), allowing for unambiguous recovery. This disambiguation could be used to recover multiple signals simultaneously given a relatively sparse input spectrum. We further note that for timing-sensitive applications in which this frequency instability is unacceptable, the microcomb can be servo-stabilized.

We have demonstrated a dual comb RF photonic system for downconversion of signals in the 3.6–18 GHz band, which can potentially serve as a front end for low-bandwidth, high-resolution electronics. Additional system improvements can be achieved using a higher-gain LNA before the IM, and higher bandwidth modulators (>40 GHz) in the EO comb. Furthermore, beyond the obvious improvement possible in size and weight, on-chip integration can offer additional system-level benefits. First, advances in thin film lithium niobate modulators offer gains in bandwidth and half-wave voltage, V_π (e.g., Ref. [25]). Second, system integration could significantly improve insertion loss—in this work, we suffer >4 dB for the pulse shaper and ~ 3 dB per modulator, but recent results have achieved ~ 1 dB on-chip insertion losses for integrated modulators [25], and ~ 40 GHz modulator bandwidth could allow us to remove the pulse shaper from our system entirely. Finally, the low conversion efficiency of Kerr solitons is a limitation that can be improved using "dark pulses" in the normal-dispersion regime, boasting efficiencies one to two orders of magnitude better than shown here [26]. This lower loss and more efficient use of power may one day circumvent the need for EDFAs. Additionally, as the RF gain in such links is proportional to P_{LO}/V_π^2 [27], substantial improvements in gain are expected. As a result of its potential for future on-chip deployment, reduced complexity through use of a single BPD, and disambiguation capability, we believe this system could be promising for applications such as mobile signals intelligence or multi-band 5G backhaul systems [28].

Funding. National Science Foundation (1809784-ECCS); U.S. Naval Research Laboratory (N00173-18-S-BA01); Air Force Office of Scientific Research (FA9550-19-1-0250); Schweizerischer Nationalfonds zur Förderung der Wissenschaftlichen Forschung (176563 (BRIDGE)); The College of Engineering Research Center at KSU; National Defense Science and Engineering Graduate.

Acknowledgments. Thanks to Anton Lukashchuk for helpful comments on the manuscript. Portions of this work were presented at CLEO 2022, paper number STh5M.7.

Disclosures. The authors declare no conflicts of interest.

Data availability. Data underlying the results presented in this paper are not publicly available at this time but may be obtained from the authors upon reasonable request.

REFERENCES

1. R.H. Walden, *Encyclopedia of Computer Science and Engineering* (Wiley2008), 126.
2. A. Khilo, S.J. Spector, and M.E. Grein, *et al.*, Opt. Express **20**, 4454 (2012).
3. C. Deakin and Z. Liu, Opt. Lett. **45**, 173 (2020).
4. A. Lukashchuk, J. Riemensberger, J. Liu, P. Marin-Palomo, M. Karpov, C. Koos, R. Bouchand, and T.J. Kippenberg, in *European Conference on Optical Communication (ECOC)* (IET, 2019) (p. 1).
5. X. Xie, Y. Dai, K. Xu, J. Niu, R. Wang, L. Yan, and J. Lin, IEEE Photonics J. **4**, 1196 (2012).
6. D. Fang, D. Drayß, G. Lihachev, P. Marin-Palomo, H. Peng, C. Füllner, A. Kuzmin, J. Liu, R. Wang, V. Snigirev, A. Lukashchuk, M. Zhang, P. Kharel, J. Witzens, C. Scheytt, W. Freude, S. Randel, T. J. Kippenberg, and C. Koos, in *European Conference on Optical Communication (ECOC)* (2021) p. 1.
7. Y. Li, N. Kuse, and M. Fermann, Opt. Lett. **43**, 1491 (2018).
8. S. A. Diddams, J. Opt. Soc. Am. B **27**, B51 (2010).
9. A. J. Metcalf, V. Torres-Company, D. E. Leaird, and A. M. Weiner, IEEE J. Sel. Top. Quantum Electron. **19**, 231 (2013).
10. T. Ren, M. Zhang, C. Wang, L. Shao, C. Reimer, Y. Zhang, O. King, R. Esman, T. Cullen, and M. Loncar, IEEE Photonics Technol. Lett. **31**, 889 (2019).
11. D. Adamy, *EW 101: A First Course in Electronic Warfare* (Artech, 2001), Vol. 101.
12. T. J. Kippenberg, A. L. Gaeta, M. Lipson, and M. L. Gorodetsky, Science **361**, eaan8083 (2018).
13. B. Shen, L. Chang, J. Liu, H. Wang, Q. F. Yang, C. Xiang, R. N. Wang, J. He, T. Liu, W. Xie, J. Guo, D. Kinghorn, L. Wu, Q. Ji, T. J. Kippenberg, K. Vahala, and J. E. Bowers, Nature **582**, 365 (2020).
14. B. Stern, X. Ji, Y. Okawachi, A. L. Gaeta, and M. Lipson, Nature **562**, 401 (2018).
15. C. Xiang, J. Liu, J. Guo, L. Chang, R. N. Wang, W. Weng, J. Peters, W. Xie, Z. Zhang, J. Riemensberger, J. Selvidge, T. J. Kippenberg, and J. E. Bowers, Science **373**, 99 (2021).
16. C. Bao, L. Zhang, A. Matsko, Y. Yan, Z. Zhao, G. Xie, A. M. Agarwal, L. C. Kimerling, J. Michel, L. Maleki, and A. E. Willner, Opt. Lett. **39**, 6126 (2014).
17. W. Shieh, H. Bao, and Y. Tang, Opt. Express **16**, 841 (2008).
18. J. Liu, G. Huang, R. N. Wang, J. He, A. S. Raja, T. Liu, N. J. Engelsen, and T. J. Kippenberg, Nat. Commun. **12**, 2236 (2021).
19. H. Guo, M. Karpov, E. Lucas, A. Kordts, M. H. Pfeiffer, V. Brasch, G. Lihachev, V. E. Lobanov, M. L. Gorodetsky, and T. J. Kippenberg, Nat. Phys. **13**, 94 (2017).
20. V. J. Urick, K. J. Williams, and J. D. McKinney, *Fundamentals of Microwave Photonics* (Wiley, 2015).
21. D. M. Pozar, *Microwave Engineering* (Wiley, 2005).
22. S. R. Harmon and J. D. Mckinney, IEEE Photonics Technol. Lett. **27**, 620 (2015).
23. C. Deakin, Z. Zhou, and Z. Liu, Opt. Lett. **46**, 1345 (2021).
24. H. Chen, R. Li, C. Lei, Y. Yu, M. Chen, S. Yang, and S. Xie, IEEE Photonics J. **6**, 1 (2014).
25. P. Kharel, C. Reimer, K. Luke, L. He, and M. Zhang, Optica **8**, 357 (2021).
26. X. Xue, P. H. Wang, Y. Xuan, M. Qi, and A. M. Weiner, Laser Photonics Rev. **11**, 1600276 (2017).
27. Y. Wu, X. B. Xie, J. H. Hodiak, S. M. Lord, and P. K. L. Yu, IEEE Photonics Technol. Lett. **16**, 2332 (2004).
28. J.A. Zhang, W. Ni, J. Matthews, C.K. Sung, X. Huang, H. Suzuki, and I. Collings, in *2014 IEEE Internat. Conference on Comm. Workshops (ICC)* (2014), p. 592).